PHYSICAL REVIEW D VOLUME 26, NUMBER 11 1 DECEMBER 1982

Transverse-momentum distributions of massive lepton pairs produced in hadronic collisions

C. Bourrely and P. Chiappetta
Centre de Physique Théorique, Centre National de la Recherche Scientifique, Luminy, Case 907, F-13288 Marseille Cedex 9, France

J. Soffer*
Institut de Physique Nucléaire, Université de Lausanne, Dorigny, Switzerland
(Received 4 August 1981; revised manuscript received 10 February 1982)

We study the transverse-momentum distributions of lepton pairs produced in hadronic collisions, in the framework of the massive-quark model. Its expectations are compared with the available experimental data at energies of Fermilab and CERN SPS. We find that our results are in fairly good agreement with the data for p and π^- induced reactions. Predictions for $\bar{p}p$ collisions and comparison with QCD are also given.

I. INTRODUCTION

The transverse-momentum distribution of a highly virtual photon γ^* of mass M produced in hadronic collisions at high energy is an important test of theoretical ideas on the production mechanism. In the classical Drell-Yan model[1] based on the parton picture, the outgoing γ^* which materializes into a lepton pair comes from a quark-antiquark annihilation and has a small transverse momentum resulting from the "primordial" transverse momentum of the constituents inside the incoming hadrons. In contrast, one observed that the γ^*'s are produced with a large transverse momentum $p_\perp$ (Ref. 2) and this experimental fact is interpreted in perturbative quantum chromodynamics (QCD) as an evidence for the emission of hard gluons carrying a large $p_\perp$ which must balance that of the γ^*. First-order QCD calculations[3] gave a reasonable description of the $p_\perp$ spectrum, but these attempts must face at least two main difficulties. Firstly, since the cross section diverges like $p_\perp^{-2}$ for small $p_\perp$, due to infrared singularities, one has to regularize with an *ad hoc* infrared cutoff before applying this approach for $p_\perp < 1$ GeV/c. In this region one should use explicit asymptotic resummation formulas[4] which are promising; more precisely one must include the effects of soft-gluon emission,[5] which somehow improve the agreement of the $p_\perp$ distribution with the data. Secondly, for cross sections integrated over the $p_\perp$ spectrum, if the structure functions of the constituents are known from deep-inelastic scattering data, one can predict the absolute normalization of the cross section, but the prediction fails by roughly a factor of 2, called the K factor.[6] This discrepancy is due to the importance of next-to-leading logarithms which have been calculated in several recent papers.[7] It was found that these terms are typically as large as 80%, so clearly it becomes hard to legitimate the validity of perturbative expansion in QCD, unless one can produce a strong argument to handle higher-order terms as suggested by large infrared effects.[8] In addition to these higher-order contributions, there are also higher-twist QCD terms, associated with coherence effects of hadronic bound states, which introduce a further complication in the detailed interpretation of the data. A direct consequence of these effects is the fact that, in the reaction $\pi^- N \to \gamma^* X$, the virtual photon γ^* has a longitudinal polarization when its longitudinal momentum fraction approaches $+1$.[9] This is in agreement with experimental observation.[10] Before claiming one has a reliable confirmation of the success of QCD from lepton-pair production data, more progress remains to be done, in particular, concerning higher-order corrections and resummation of soft gluons. So we wish to propose a different theoretical framework to study this specific aspect of hadronic collisions. We shall adopt an approach based on the massive-quark model (MQM) which was proposed several years ago.[11] In this physical picture, confinement of hadronic constituents is built in from the begin-

ning by imposing that hadronic matter can be found only in finite space-time regions. This bag model, which is distinct from the so-called MIT bag model,[12] becomes more specific when combined with geometrodynamical principles and yields, in particular, the spectrum of hadronic states lying approximately on linear Regge trajectories.[13] Having constructed these states, one is able to describe their interactions by means of weak and electromagnetic currents coupled directly to quarks and to give a satisfactory description of fundamental processes such as deep-inelastic phenomena.[14–16] Some aspects of lepton-pair production have also been analyzed recently in the MQM, but transverse-momentum distributions were ignored.[17]

The paper is organized as follows. In Section II, we will consider the notion of elongated quark-antiquark structure which plays a central role in large-$p_\perp$ physics and we will discuss its main properties. Section III is devoted to the explicit calculation of the $p_\perp$ spectrum within the assumptions of the MQM. Our results will be compared with experimental data for p and π^- induced reactions on nuclear targets in Sec. IV. We shall also give predictions for the reaction $\bar{p}p \to \bar{l}lX$ at CERN SPS energies. Comparison with QCD and concluding remarks will be made in Sec. V.

II. THE ELONGATED QUARK-ANTIQUARK STRUCTURE: DEFINITION AND BASIC PROPERTIES

In high-energy reactions, where high-mass hadronic states are produced, the concept of elongated quark-antiquark structure (S) is very relevant for the description of the structure of final states[18,19] and also, as we will see, for the calculation of the $p_\perp$ spectrum in lepton-pair production. In this section we shall briefly recall what is S and we shall discuss its main properties.

Let us first consider the wave function $\psi(p,x_q,x_{\bar{q}})$ of a $q\bar{q}$ system of total four-momentum p, where x_q and $x_{\bar{q}}$ are the coordinates of the quark q and of the antiquark $\bar{q}$. In the MQM approach one imposes on ψ the three following requirements: (i) translation invariance, (ii) quark confinement in a finite space-time "bag" region, and (iii) free quark motion at short distances. ψ is therefore a function of $x=x_q-x_{\bar{q}}$ and its Fourier transform, i.e., the wave function in momentum space of mesons of high mass M is given by

$$\psi_{mnl}(p,k)=N_{nl}(M)\delta_{R^2}(\tfrac{1}{2}(p_q{}^2+p_{\bar{q}}{}^2)) \times\delta_{R^2}(\tfrac{1}{2}(p_q{}^2-p_{\bar{q}}{}^2))Y_l^m(\Omega_{\vec{k}}) , \quad (1)$$

where $p_q=p/2+k$, $p_{\bar{q}}=p/2-k$, l is the orbital angular momentum of the $q\bar{q}$ system, and n is the radial quantum number. R is related to the radius of the mesonic bag and from the low-mass meson families one obtains $R^2\simeq 2$ GeV^{-2}.[13] For large masses, the spectrum is characterized by the relation

$$M^2\simeq\frac{\pi}{R^2}(2n+l) , \quad (2)$$

so one obtains an infinite set of linear and parallel Regge trajectories without odd daughters. The function $\delta_{R^2}(z)$ is a "fat function" which becomes a Dirac δ function in the limit where R goes to infinity. A very simple expression for this function is

$$\delta_{R^2}(z)\simeq\frac{1}{\pi}\frac{\sin R^2 z}{z} .$$

$Y_l^m(\Omega_{\vec{k}})$ is a normalized spherical harmonic depending on the angular variables of $\vec{k}$. Finally, $N_{nl}(M)$ is a normalization factor depending on the mass and spin of the $q\bar{q}$ system. When one couples this meson to the electromagnetic current, $N_{nl}(M)$ can be calculated by imposing the normalization of the meson charge form factor at zero momentum transfer. In this procedure one must consider two contributions to the form factor as shown in Fig. 1. The first term [Fig. 1(a)] is the vector-meson

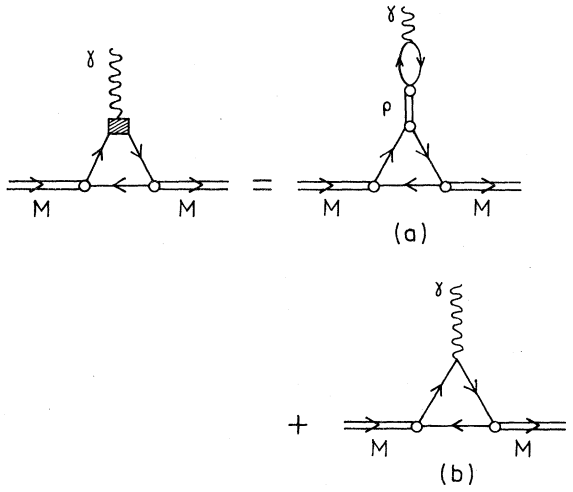

FIG. 1. The two couplings of a meson M to the photon: (a) the vector-meson coupling with ρ dominance; (b) the direct coupling.

coupling where one uses ρ dominance and the second term [Fig. 1(b)] is the direct coupling of the current to quarks. As a result of this calculation,[13] one finds that for a given high-mass value M, all the meson states such that $l > l_0$ with $l_0 = M/m_\rho$, m_ρ being the ρ mass, have a small wave function. In other words, $q\bar{q}$ states with large angular momentum are suppressed and this is a natural expectation if strong interactions have a finite range. From the meson states such that $l < l_0$, one can construct the following superposition of wave functions:

$$|p,M,\Omega_0\rangle = \frac{1}{{l_0}^2} \sum_{l=0}^{l_0} \sum_n \sum_{m=-l}^{+l} Y_l^{-m}(\Omega_0)\psi_{nlm}(p,k) , \tag{3}$$

where the sum over n must take Eq. (2) into account.

Such a coherent mesonic state, called an elongated quark-antiquark structure (S) characterized by the direction Ω_0, describes a universal cylindric structure produced in all high-energy collisions. S is not stable and shortly after it is produced it will decay into states whose properties are determined by the three-meson vertex which appeared already in Fig. 1(a). The dominant decay mode is[13,18]

$$S_1 \to S_2 + M_V , \tag{4}$$

i.e., a high-mass S produces another high-mass S and a low-mass meson M_V. This low-mass meson is a vector meson whose coupling is dominant according to the MQM.[13,19] This feature of the model leads in particular to the fact that almost all pseudoscalar mesons are produced at high energy from resonance decay, in agreement with experimental data. The iteration of this transition mode leads to the picture where one gets a linear decay chain of the initial highly excited state. The transition amplitude can be calculated explicitly from the meson wave functions and from the three-meson vertex. If one considers the special case where the S is made of light quarks and the produced low-mass meson M_V is a vector meson, the decay distribution is characterized by[19]

$$K(x) = n_k \frac{(2x-1)(1-x)}{x^2} \theta(x - \tfrac{1}{2}) , \tag{5}$$

n_k is a normalization factor determined from the decay width, and $x = 2E_{M_V}/M$, where E_{M_V} is the energy of the vector meson M_V and M is the mass of the initial S. Here, unlike in Ref. 19, we are neglecting the transverse momentum of the vector meson M_V with respect to the direction of the initial S. This approximation will be justified in our case since according to Ref. 19 the average $p_\perp$ of the produced vector meson is $\langle p_\perp \rangle \sim 0.45$ GeV. The quark of the S which has emitted a vector meson will, in general, change direction and so will the S. Therefore, at any step in the decay chain there is a nonvanishing "tilting" probability that the S rotates by an angle θ and continues its canonical linear decay chain in the new direction. The probability for tilting an S of large mass M by an angle θ has been calculated in Ref. 19 and reads in the rest frame of the S,

$$\frac{dN}{d\cos\theta} = \frac{(M\Gamma)}{\pi M^2} \frac{1}{(3-2\cos\theta)^2} \frac{1}{[1-\cos\theta + (m_\rho{}^2/M^2)(2-\cos\theta)]} + \frac{2m_\rho{}^4}{M^4} \frac{1}{[1-\cos\theta + (m_\rho{}^2/M^2)(2-\cos\theta)]^3} , \tag{6}$$

where $(M\Gamma)$ is the total width of the S and we shall take as in Ref. 19 $(M\Gamma) \simeq 4$ GeV.^{2} When the angle θ is different from zero the first term dominates over the second one for large values of M and it goes like $1/M^2$.

The decay and the tilt of S are the main dynamical inputs one invokes, in the framework of the MQM, to describe the origin of jets in e^+e^- annihilation[19] or multiparticle events at large $p_\perp$, together with the fact that the S decay is dominated by vector-meson emission. For studying transverse-momentum distributions in lepton-pair production, we will use the same ingredients in addition to the probability for producing an S which is related to the structure functions measured in deep-inelastic scattering. Let us emphasize that here again we will not consider the emission of pseudoscalar mesons by an S because it would lead to a Drell-Yan cross section roughly one order of magnitude lower than experimentally observed.

III. THE $p_\perp$ SPECTRUM

Let us consider the process

$$h_1 h_2 \to (l^+ l^-) + X \tag{7}$$

where a massive lepton pair $(l^+ l^-)$ of mass M is produced with transverse momentum $p_\perp$ and rapidity y. The cross section $(d\sigma/dM\,dy\,dp_\perp{}^2)\,|_y$ for this reaction, at a fixed value of y, is calculated in the MQM by means of the two diagrams depicted in Fig. 2. The two hadrons h_1 and h_2 are emitting a quark and an antiquark which make the initial S. This S will decay according to (4) but, as mentioned above, it has a certain probability to tilt by an angle θ^*, this probability being large when the mass of the S is small [see Eq. (6)]. The quark q and the antiquark $\bar{q}$ of the S before tilting carry the longitudinal-momentum fractions x_1 and x_2 and the transverse momenta p_q and $p_{\bar{q}}$. After tilting the S has a last decay step where it produces the timelike photon giving the observed lepton pair $(l^+ l^-)$ and a vector meson which is assumed to have no transverse momentum and a longitudinal-momentum fraction x. Two diagrams appear in Fig. 2 because for symmetry reasons one should be able to permute the vector meson and the photon.

According to the MQM rules the diagram in Fig. 2(a) gives the following contribution to the cross section at a fixed value of the rapidity y of the photon $y=\frac{1}{2}\ln[(Q_0+Q_L)/(Q_0-Q_L)]$,

$$\frac{d\sigma}{dM\,dy\,dp_\perp{}^2}=\frac{8\pi\alpha^2}{9M}[F_{q\bar{q}}(M,y,p_\perp)+(q\leftrightarrow\bar{q})]\lambda^{-1}F_\lambda(M^2)\,, \tag{8}$$

where

$$F_{q\bar{q}}(M,y,p_\perp)=\sum_f e_f{}^2\int dx_1 dp_q{}^2 \tilde{f}_q{}^{h_1}(x_1,p_q)\int dx_2 dp_{\bar{q}}{}^2 \tilde{f}_{\bar{q}}{}^{h_2}(x_2,p_{\bar{q}})$$
$$\times\int\frac{dx}{x}K(x)\int d\cos\vartheta^*\frac{dN}{d\cos\theta^*}\delta^{(4)}(Q-(p_1'+p_2'))\,. \tag{9}$$

The first factor in Eq. (8) is very general of inclusive production of the $(l^+ l^-)$ pair through a virtual photon. Before we discuss, in more detail, the function $F_{q\bar{q}}$ in Eq. (9) and how to calculate it, let us first make some comments on the normalization of the cross section which is completely fixed by λ^{-1} and $F_\lambda(M^2)$ as in Ref. 17. The factor λ^{-1} can be evaluated by assuming Pomeron dominance in the hadronic tensor $W_{\mu\nu}$. It is also related to the ratio R in e^+e^- annihilation and in the MQM[13] one has $\lambda^{-1}=\pi/4$, whereas in the parton model $\lambda^{-1}=1$. As we have seen above (see Fig. 1), the coupling of a real photon to the $q\bar{q}$ pair involves two terms. This is also the case for a timelike photon, so the usual direct coupling which occurs in Fig. 2 will be multiplied by the amplitude

$$A(M^2)=1+i\lambda-\frac{\lambda}{\pi}\ln\left[\frac{M^2}{M_0{}^2}\right]\,,$$

where M_0 is a parameter related to a subtraction in the dispersion relation used to calculate the above amplitude. The function $F_\lambda(M)$ which appears in the cross section [Eq. (8)] is the modulus square of

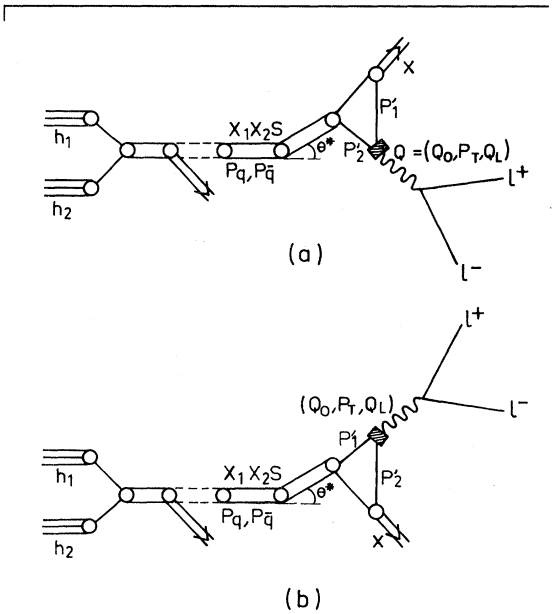

FIG. 2. Two lines joining two circles represents an elongated $q\bar{q}$ structure (S). Two lines with an arrow on them represents the emission of a vector meson. The vertex where θ^* appears represents the tilt of the S. (a) Corresponds to the emission of the vector meson by the quark. (b) Respectively, the antiquark.

$A(M^2)$,

$$F_\lambda(M^2)=\lambda^2+\left[1-\frac{\lambda}{\pi}\ln\left[\frac{M^2}{{M_0}^2}\right]\right]^2 . \tag{10}$$

We have chosen $M_0=5$ GeV for best agreement with the data, but if you put a smaller value, i.e., $M_0=2$ GeV, in the range of mass of lepton pair we are interested in, the cross section will change at most by 20%, which is the uncertainty in the normalization of the experimental data.

Let us now come back to $F_{q\bar{q}}$ defined by Eq. (9). For the structure functions $\tilde{f}_i^h$ we assume the following parametrization:

$$\tilde{f}_i^h(x,p_i)=\frac{\mu}{\pi}e^{-\mu {p_i}^2}f_i^h(x) \quad (i=q,\bar{q}) , \tag{11}$$

where the $f_i^h(x)$ are the structure functions extracted from the MQM analysis of deep-inelastic scattering[14,15] that we shall give in Appendix A.

In (11) we have assumed a simple form for the transverse-momentum distribution of partons inside the S. The S being a universal hadronic structure, the mean transverse momentum can be extracted from the Monte Carlo analysis of the S decay in e^+e^- annihilation. It is found that this mean value grows linearly with the logarithm of the center-of-mass energy of the initial $q\bar{q}$ pair. So for the reaction (7) with total squared energy s we have

$$\langle p_i\rangle = a+b\ \ln(\bar{x}_q^{h_1}\bar{x}_{\bar{q}}^{h_2}s) \tag{12}$$

where $\bar{x}_q$ and $\bar{x}_{\bar{q}}$ are the average energy fractions carried by q and $\bar{q}$ which depend on the parent hadrons. A reasonable choice from present knowledge of hadron structure is

$$\begin{aligned} &\bar{x}_q^p=\tfrac{1}{5},\ \ \bar{x}_{\bar{q}}^p=\tfrac{1}{10} ,\\ &\bar{x}_q^{\bar{p}}=\tfrac{1}{10},\ \ \bar{x}_{\bar{q}}^{\bar{p}}=\tfrac{1}{5} ,\\ &\bar{x}_q^\pi=\bar{x}_{\bar{q}}^\pi=\tfrac{1}{3} . \end{aligned} \tag{13}$$

From e^+e^- annihilation[20] b is equal to 0.15 GeV. The intrinsic average transverse momentum a is taken equal to 0.29 GeV, a value which is independent of the initial hadrons. The determination of μ which appears in Eq. (11) follows immediately from the knowledge of Eq. (12).

The tilting probability $dN/d\cos\theta^*$ is normalized in such a way that by integrating the cross section over ${p_\perp}^2$ one recovers the well-known scaling law for $M^3(d\sigma/dM)$.

The explicit expression of the Dirac function $\delta^{(4)}(Q-(p_1'+p_2'))$, where Q is the four-momentum of the massive photon and p_1' (p_2') is the four-momentum of the quark (antiquark), will be given in Appendix B. This quadridimensional Dirac function allows us to eliminate some of the integrations which appear in (9). From Eqs. (B7) and (B8), we can integrate over p_q and $p_{\bar{q}}$ and from (B6) and (B9) over x_1 and x_2, whose values are

$$x_{1,2}=\frac{2(Q_0\pm Q_L)}{\sqrt{s}\,(2-x\mp x\cos\theta^*)} . \tag{14}$$

Finally, it remains to integrate over x and $\cos\theta^*$ in a certain kinematic domain obtained from the requirements $0\le x_{1,2}\le 1$. After some calculations Eq. (9) becomes

$$\begin{aligned} F_{q\bar{q}}(M,y,p_\perp)=\frac{\mu}{\pi}\int_{x_{\max}/2}^{x_{\max}}\frac{dx}{x}K(x)\int d\cos\theta^*\frac{dN}{d\cos\theta^*}\frac{8\pi^2 A}{[(1-x)+\frac{1}{4}x^2\sin^2\theta^*]s}\\ \times\exp\left[-\mu A\left[{p_\perp}^2+\frac{x_1x_2sx^2}{4}\sin^2\theta^*\right]\right]I_0(\,|\mu A(x_1x_2s)^{1/2}x\sin\theta^* p_\perp|\,)\\ \times\sum_f e_f^2 f_q^{h_1}(x_1)f_{\bar{q}}^{h_2}(x_2) , \end{aligned} \tag{15}$$

where

$$A=\frac{1}{\left[1-\frac{x}{2}(1+\cos\theta^*)\right]^2+\left[1-\frac{x}{2}(1-\cos\theta^*)\right]^2} .$$

I_0 is the zeroth-order Bessel function of imaginary argument. $x_{\max}$ is the maximal energy fraction carried by the vector meson in the last step of the S decay,

$$x_{\max}=1-\frac{(Q_0+|\,Q_L\,|)}{\sqrt{s}} .$$

The diagram in Fig. 2(b) gives a contribution to $F_{q\bar{q}}(M,y,p_\perp)$ analogous to Eq. (15), but the values of x_1 and x_2 are in this case

$$x'_{1,2}=\frac{2}{\sqrt{s}}\left[\frac{Q_0\pm Q_L}{2-x\pm x\cos\theta^*}\right].$$

We have now everything to compute the $p_\perp$ spectrum for the reaction of Eq. (7). Of course, the expression for $F_{q\bar{q}}$ is not a simple one and to evaluate the cross section we will have to perform the last two integrations by computer.

IV. RESULTS AND COMPARISON WITH EXPERIMENTAL DATA

We have compared our results with experimental data obtained from proton beams on platinum targets[2] [Columbia–Fermilab–Stony Brook (CFS) collaboration] and negative pions on platinum targets[21] (CERN NA3 collaboration). The fact that the target is a complex nuclei requires the use of the structure functions of both protons and neutrons with the appropriate ratio.

In the case of the CFS experiment we have calculated the invariant cross section at a fixed rapidity y (Ref. 22) by integrating Eq. (8) over several mass bins divided by the factor π. In Fig. 3 we show our $p_\perp$ spectrum for $\langle y\rangle=0.03$ and $p_{\rm lab}=400$ GeV/c. The agreement of the theoretical curves with the data for each mass bin (from 5 to 12 GeV) is very good both in shape and normalization for the whole $p_\perp$ range. Figures 4 and 5 exhibit the same comparison at different $p_{\rm lab}$ and $\langle y\rangle$ and show an equally good agreement between theory and experiment for small and intermediate $p_\perp$. For large $p_\perp$ the cross section behaves like a Gaussian. However, the main decay mode of the S we have considered [Eq. (4)] in this paper is only dominant for small $p_\perp$ ($p_\perp \lesssim 3-4$ GeV/c). For higher $p_\perp$, which has not yet been investigated experimentally, one should also consider the mechanism $S\to S_1+S_2$ where an elongated $q\bar{q}$ structure S gives rise to two heavy objects S_1 and S_2. This new decay mode will lead to a higher cross section for high $p_\perp$ as in the case of e^+e^- annihilation (see Ref. 19).

In the case of the NA3 collaboration the cross-section data shown in Fig. 6 are for $(1/p_\perp)d^2\sigma/dM\,dp_\perp$, where one has integrated over the rapidity range of the experiment $-0.4\le y\le 1.2$. To compare with these data we have calculated the expression

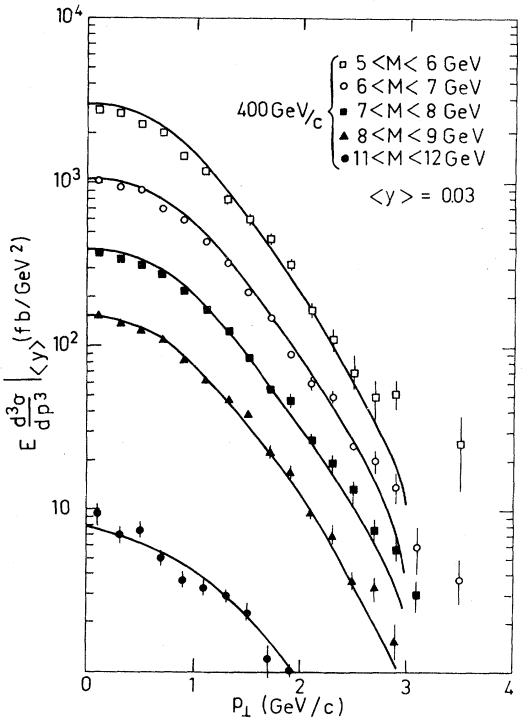

FIG. 3. The invariant cross section vs $p_\perp$ at $p_{\rm lab}=400$ GeV/c and $\langle y\rangle=0.03$ (data from Ref. 2).

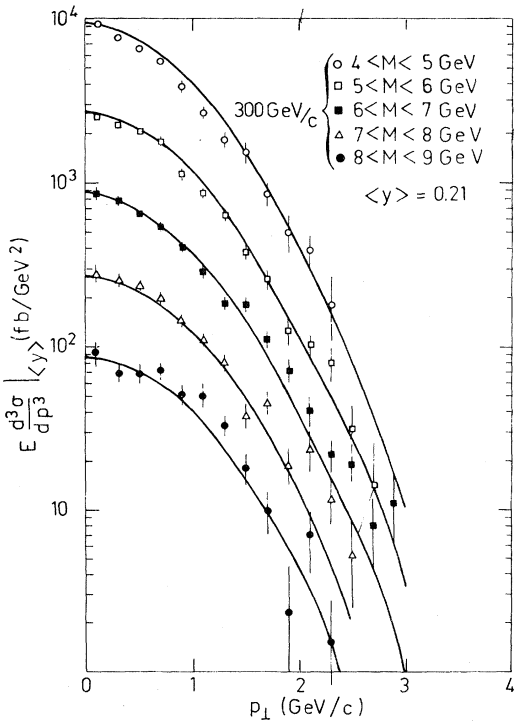

FIG. 4. The invariant cross section vs $p_\perp$ at $p_{\rm lab}=300$ GeV/c and $\langle y\rangle=0.2$ (data from Ref. 2).

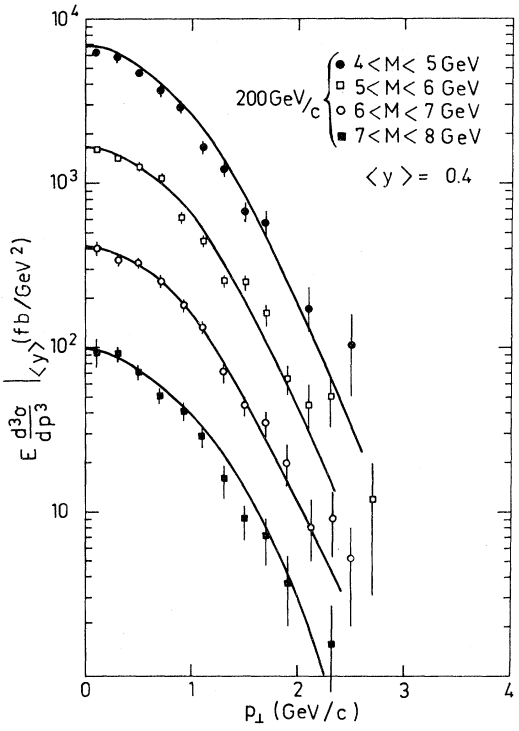

FIG. 5. The invariant cross section vs $p_\perp$ at $p_{\rm lab}=200$ GeV/c and $\langle y\rangle=0.4$ (data from Ref. 2).

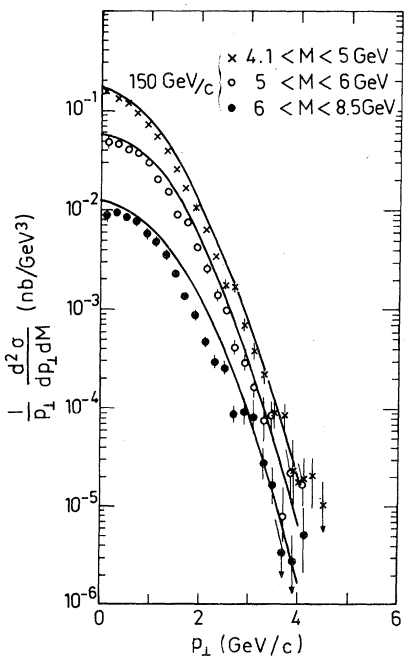

FIG. 6. The cross section $(1/p_\perp)(d^2\sigma/dM\,dp_\perp)$ vs $p_\perp$ at $p_{\rm lab}=150$ GeV/c (data from Ref. 21).

$$\left.\frac{2\pi}{\Delta M}E\frac{d^3\sigma}{dp^3}\right|_{y=0},$$

where ΔM is the mass interval and we have checked that the integration in the above rapidity range of the cross section $d^2\sigma/dM\,dy$ is well approximated by its value at $y=0$. As shown in Fig. 6 the theory is in fairly good agreement with the data on a rather large $p_\perp$ interval. However, the theoretical curves are slightly above the data points, but for a better comparison it would be more suitable to have the invariant cross section $E\,d^3\sigma/dp^3|_y$ in small rapidity bins as in the case of the CFS collaboration. In Fig. 7(a) we plot the

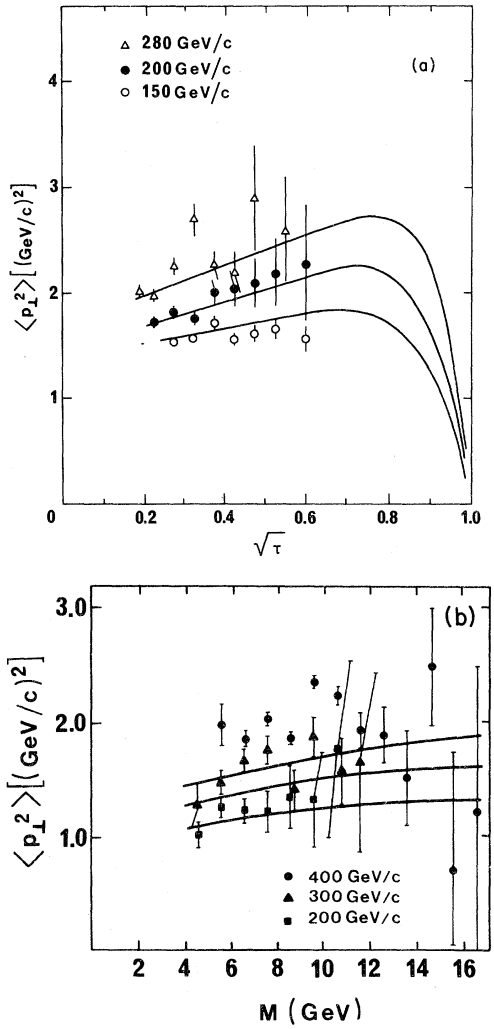

FIG. 7. (a) The mean-squared transverse momentum $\langle p_\perp{}^2\rangle$ in πN collisions at $p_{\rm lab}=150$, 200, and 280 GeV/c (data from Ref. 21) versus the variable $\sqrt{\tau}=M/\sqrt{s}$. (b) The mean-squared transverse momentum $\langle p_\perp{}^2\rangle$ in pN collisions (CFS) at $p_{\rm lab}=200$, 300, and 400 GeV/c (data from Ref. 2) versus the lepton-pair mass.

mean-squared transverse momentum $\langle p_\perp{}^2\rangle$ vs the lepton-pair mass at three different energies for $\pi^- N$ collisions. The observed rise is well reproduced by our model in the limited range of $\sqrt{\tau}$. Due to the complicated expression of $F_{q\bar{q}}$ given in Eq. (15), we could not anticipate the linear rise we have obtained up to $\sqrt{\tau}\sim 0.7$ or so. The only thing we can say is that if $\langle p_\perp{}^2\rangle$ were flat at fixed energy this would mean that the cross section factorizes as $f(p_\perp)\times g(M)$. In our case obviously we do not have this factorization property. As expected the curves in Fig. 7(a) fall to zero as $\sqrt{\tau}\to 1$. This is a kinematical constraint because when we reach the phase-space boundary $M\sim\sqrt{s}$, the maximum $p_\perp$ value must be very small as $\langle p_\perp{}^2\rangle$. In Fig. 7(b) we plot the mean-squared transverse momentum $\langle p_\perp{}^2\rangle$ vs the lepton-pair mass for pN collisions (CFS data) at three different energies. We find in this case that our theoretical curves, flatter than in the previous case, are in acceptable agreement with the data at 200 GeV/c. However, we do not reproduce the $p_{\rm lab}$ dependence of $\langle p_\perp{}^2\rangle$ at fixed τ since the 300 and 400 GeV/c data are above our curves. For 400 GeV/c this reflects the fact that in the $p_\perp$ distribution shown in Fig. 3, we are missing the experimental points for $p_\perp \gtrsim 3$ GeV/c. The difference of behavior of $\langle p_\perp{}^2\rangle$ in $\pi^- N$ and pN collisions is due to the different shapes of the $p_\perp$ distributions which are related to the mean transverse momentum of the partons inside the elongated $q\bar{q}$ structure [see Eq. (12)].

There are also some CERN ISR data[23] on the $p_\perp$ distribution which are of course less accurate than the fixed target data previously mentioned. At these very high energies, we predict from Eq. (12) a lower slope of the $p_\perp$ spectrum in agreement with experimental observation.

V. COMPARISON WITH QCD AND CONCLUDING REMARKS

Clearly the MQM is one particular model, but so far the QCD approach is also in rather good agreement with the data. Therefore we feel that it is worth thinking about how future data can discriminate between these two challenger models. This is what we shall discuss now. We will examine successively three specific features of the Drell-Yan pairs where the two models give distinct predictions, that is the K factor at high lepton masses M, the rise of $\langle p_\perp{}^2\rangle$ with M in $\pi^- N$ collisions, and the $p_\perp$ spectrum in $\bar{p}p$ collisions.

Concerning the K factor, QCD predicts that it is approximately constant with the mass M and with the rapidity y of the lepton pair over the kinematic region investigated so far. For very large values of the lepton-pair mass when we reach the boundary of the phase space, it is essential to use the exact kinematic for the soft-gluon transverse momentum. As a consequence, QCD predicts in this region, not yet explored by experiments, a fast rise, typically from 2.5 to 4 for $0.7<\tau<0.9$ in πp collisions as shown in Fig. 8. In the MQM, the K factor is given by Eq. (10), so the M dependence is logarithmic and it does not exhibit a sudden rise in the limit $\tau\to 1$ whatever the value of M, as shown in Fig. 8. Moreover, K is universal and it does not depend on the initial hadrons. The two models can be certainly discriminated for large values of τ, namely for $\tau>0.8$, but we do not know if, in a near future, experiments will be able to allow a conclusive test from this K factor.

Let us now discuss the transverse-momentum properties of lepton pairs. First-order QCD calculations[3] do not provide a very good description of the p_T spectrum due to the following reasons. First, the unregularized cross section, which is infrared divergent at small p_T, should agree with the data at high p_T. This is not the case because it gives a result ten times below the data for $\pi^- N$ collisions. Second, if one regularizes it by introducing an intrinsic transverse momentum, its average value has to be rather large, namely of the or-

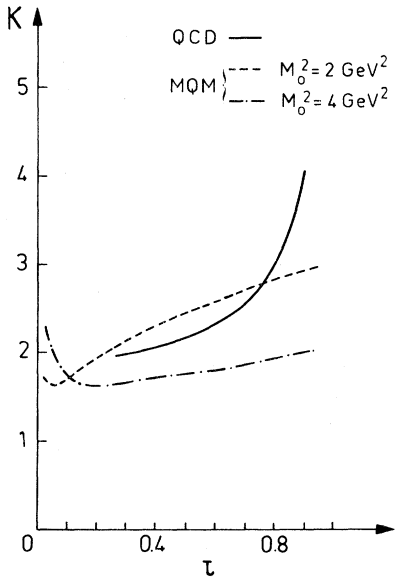

FIG. 8. The K factor for πp collisions in QCD (solid curve, Ref. 8) and MQM (dashed and dot-dashed curves, Ref. 17).

der of 1 GeV. For small and intermediate p_T, the data are well understood by resumming large terms like $\alpha_s{}^n \ln^{2n}(M^2/p_T{}^2)$ (α_s being the QCD running coupling constant) as emphasized by many authors.[5,24] Even without considering fully the nonleading-logarithm contributions,[25] the use of the exact kinematics for the gluon transverse-momentum phase space at the leading-logarithm level improves considerably the phenomenological analysis, bringing theory in good agreement with data as can be seen in Ref. 26. It is interesting to note that in this case the parton intrinsic transverse momentum is reduced to a moderate value, typically $\langle p_T{}^2\rangle \sim 0.3-0.4$ GeV^2. Let us now consider the high $-p_T$ region, i.e., $p_T > 2-3$ GeV/c. The failure of first-order calculations in this region is certainly due to the fact that the p_T values presently accessible to experiments are too small to be sensitive to hard gluons. Here both accurate data, soon available, and higher-order hard annihilation and Compton calculations should help clarify the situation. This is strongly supported by recent second-order calculations[27] of hard annihilation terms which multiply the first order by roughly a factor 2, in better agreement with data only for $\pi^- N$ collisions at $p_T \geq 3$ GeV/c.

In the MQM, as we have seen, the relevant concept for the p_T dependence of the lepton pair is a multivector meson emission during the decay of the elongated quark-antiquark structure (S) which increases, at each decay step, the transverse momentum of the initial quark-antiquark pair. For small and intermediate p_T spectrum the agreement is very good. A rather small value of the intrinsic transverse momentum ($\langle p_T\rangle_{\text{intr}} \sim 0.3$ GeV) is required in this analysis.

Concerning the rise of the mean squared transverse momentum with the lepton mass M, the slope is important for small masses in QCD whereas it is quite flat in the MQM as shown in Fig. 9. Nevertheless, present data are not accurate enough to discriminate between the two models. At higher lepton masses the behavior is completely different. The MQM predicts a rise of $\langle p_T{}^2\rangle$ with

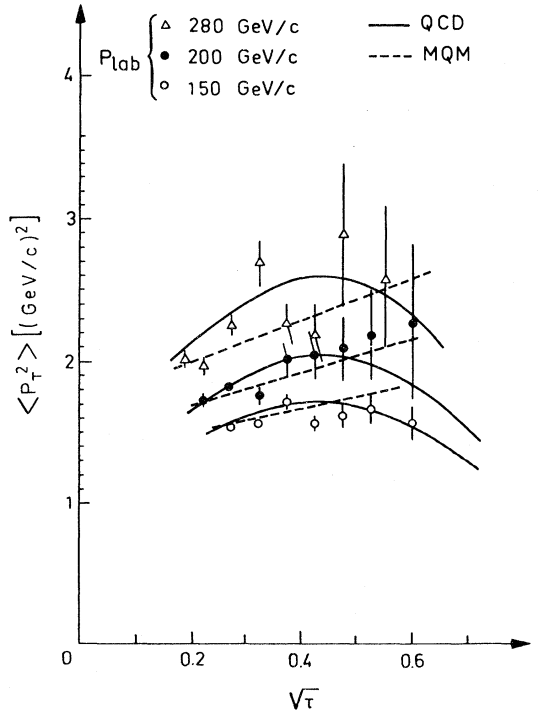

FIG. 9. The mean-squared transverse momentum $\langle p_\perp{}^2\rangle$ for $\pi^- N$ collisions. Solid curve: QCD prediction (Ref. 26). Dashed curve: MQM prediction.

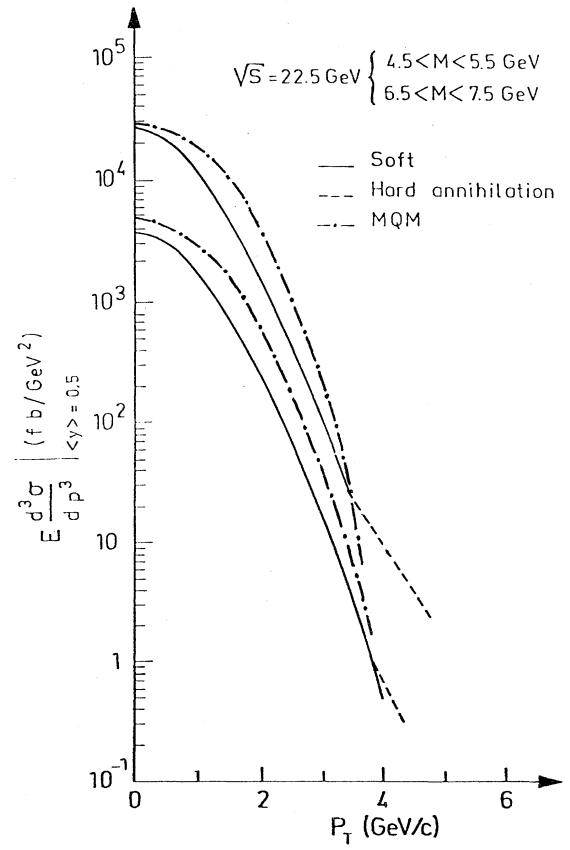

FIG. 10. Predictions for the invariant cross section $Ed^3\sigma/dp^3$ for $p\bar{p}$ collisions at $\sqrt{s} = 22.5$ GeV and $\langle y\rangle = 0.5$. Solid curve: soft QCD contribution (Ref. 26). Dashed line: hard annihilation QCD, first- and second-order contributions (Ref. 26). Dot-dashed curve: MQM prediction.

$\sqrt{\tau}$ up to $\sqrt{\tau} \sim 0.7$ or so, whereas in QCD $\langle p_T^2 \rangle$ falls down already at $\sqrt{\tau} \gtrsim 0.5$, so new data at higher masses[28] should definitely discriminate between the two approaches. Another way to do that is to look at the p_T distributions in $p\bar{p}$ collisions. In Fig. 10, we see that the cross section vs p_T decreases much faster in soft multigluon emission than in the MQM. The difference is so important that experimental data in $p\bar{p}$ collisions which will be soon accessible[29] must give the answer.

In conclusion, future Drell-Yan experiments in pN, πN, and $p\bar{p}$ collisions will be able to clearly discriminate between two different high-energy models. These models lead to specific predictions for the K factor which seem rather hard to test experimentally. They predict different behavior for the mean squared transverse momentum against the lepton-pair mass M for large M, which are worth being carefully analyzed. The crucial test is certainly the transverse-momentum distribution in $p\bar{p}$ collisions.

ACKNOWLEDGMENTS

We are grateful to G. Preparata for several interesting discussions at an earlier stage of this work and to G. Valenti for informative conversations on the decay of the S. We also thank M. Le Bellac for clarifying our views on the increasing complexity of perturbative QCD. One of us (P.C.) would like to thank the Commissariat à l'Energie Atomique for financial support.

APPENDIX A: STRUCTURE FUNCTIONS

We give in this appendix the structure functions we have used for the calculation of the $p_\perp$ spectrum in Eq. (11). We take for nucleons

$$f_u^p(x)=f_d^n(x)=\tfrac{5}{3}\alpha_0(1-x)^3+6\theta_{20}\frac{(1-x)^{7/2}}{\sqrt{x}}+\tfrac{3}{2}\theta_0\frac{(1-x)^9}{x},$$

$$f_d^p(x)=f_u^n(x)=\tfrac{1}{3}\alpha_0(1-x)^3+3\theta_{20}\frac{(1-x)^{7/2}}{\sqrt{x}}+\tfrac{3}{2}\theta_0\frac{(1-x)^9}{x},$$

$$f_{\rm sea}^p(x)=f_{\rm sea}^n(x)=\tfrac{3}{2}\theta_0\frac{(1-x)^9}{x}+\theta_{10}\frac{(1-x)^7}{\sqrt{x}}$$

and for mesons

$$f_d^{\pi^-}(x)=A\frac{(1-x)^3}{3x}F(2,1,4;1-x)+C(1-x)+\frac{B}{5}\frac{(1-x)^{5/2}}{\sqrt{x}}F(1,2,\tfrac{7}{2};1-x),$$

where $F(a,b,c;z)$ is the Gauss hypergeometric function and

$$f_{\rm sea}^{\pi^-}(x)=A\frac{(1-x)^3}{3x}F(2,1,4;1-x)$$

with the following values for the parameters:

$$\alpha_0=0.1623,\quad A=0.06,$$

$$\theta_{20}=0.3671,\quad C=0.36,$$

$$\theta_0=0.2,\quad B=(1-C)/1.06.$$

$$\theta_{10}=0.0795,$$

Note that this parametrization is a refined version of the one adopted in Ref. 14 in order to describe correctly low-Q^2 SLAC data on nuclear targets.

APPENDIX B: KINEMATICS OF THE REACTION

We consider an elongated quark-antiquark structure S made of a quark-antiquark pair whose fractions of longitudinal momentum are x_q, $x_{\bar{q}}$, and transverse momentum p_q, $p_{\bar{q}}$. We define the four-momentum of quark and antiquark as

$$\tilde{p}_q=\left[\frac{\sqrt{s}}{2}x_q,p_{qx},p_{qy},\frac{\sqrt{s}}{2}x_q=p_{qL}\right],$$
$$\tilde{p}_{\bar{q}}=\left[\frac{\sqrt{s}}{2}x_{\bar{q}},p_{\bar{q}x},p_{\bar{q}y},-\frac{\sqrt{s}}{2}x_{\bar{q}}=p_{\bar{q}L}\right], \tag{B1}$$

where s is the center-of-mass energy of the incident hadrons. In the following we use the notations

$$\epsilon_q=\frac{\sqrt{s}}{2}x_q,\quad \epsilon_{\bar{q}}=\frac{\sqrt{s}}{2}x_{\bar{q}},\quad E=\epsilon_q+\epsilon_{\bar{q}},$$

$$\vec{P}=\vec{P}_L+\vec{P}_\perp=\vec{p}_q+\vec{p}_{\bar{q}},\quad M=(x_q x_{\bar{q}}s)^{1/2}.$$

Making a boost such that the elongated quark-antiquark structure S is at rest, we obtain for the quark components (in the approximation $\vec{P}\cdot\vec{p}_q \approx P_L p_{qL}$)

$$p^*_{qx}=\tfrac{1}{2}(p_{qx}-p_{\bar{q}x})-\frac{(p_{qx}+p_{\bar{q}x})P_L}{2(E+M)}\ ,$$
$$p^*_{qy}=\tfrac{1}{2}(p_{qy}-p_{\bar{q}y})-\frac{(p_{qy}+p_{\bar{q}y})P_L}{2(E+M)}\ ,$$
$$p^*_{qL}=\frac{M}{2}\ , \qquad \text{(B2)}$$
$$\epsilon^*_q=\frac{M}{2}\ ,$$

for the antiquark components

$$p^*_{\bar{q}x}=-\tfrac{1}{2}(p_{qx}-p_{\bar{q}x})+\frac{(p_{qx}+p_{\bar{q}x})P_L}{2(E+M)}\ ,$$
$$p^*_{\bar{q}y}=-\tfrac{1}{2}(p_{qy}-p_{\bar{q}y})+\frac{(p_{qy}+p_{\bar{q}y})P_L}{2(E+M)}\ ,$$
$$p^*_{\bar{q}L}=-\frac{M}{2}\ , \qquad \text{(B3)}$$
$$\epsilon^*_{\bar{q}}=\frac{M}{2}\ .$$

In the S rest frame we choose P_L along the z axis, and we tilt the S by a set of angles θ^*, φ^*. The new components of the quark are

$$p''_{qx}=-p^*_{qL}\sin\theta^*\cos\varphi^*+p^*_{qx}\cos\theta^*\ ,$$
$$p''_{qy}=-p^*_{qL}\sin\theta^*\sin\varphi^*+p^*_{qy}\cos\theta^*\ , \qquad \text{(B4)}$$
$$p''_{qz}=p^*_{q\perp}\sin\vartheta^*+p^*_{qL}\cos\theta^*\ ,$$

where

$$p^*_{q\perp}=(p^{*2}_{qx}+p^{*2}_{qy})^{1/2}\ .$$

For the antiquark we change $q\to\bar{q}$.

Let us suppose that the vector meson is emitted by the quark longitudinally and it carries a fraction x of its momentum. The resulting components of the quark are

$$\vec{p}'^{\,*}_q=(1-x)\vec{p}''_q\ ,$$
$$\epsilon'^{\,*}_q=(1-x)\epsilon^*_q\ . \qquad \text{(B5)}$$

After having tilted the S and emitted the vector meson, we make a boost to put the S in its original frame. The new components are

$$p^x_S=\frac{M}{2}x\sin\theta^*\cos\varphi^*+p_{qx}\left[1-\frac{x}{2}(1+\cos\theta^*)\right]$$
$$+p_{\bar{q}x}\left[1-\frac{x}{2}(1-\cos\theta^*)\right]\ , \qquad \text{(B6)}$$

$$p^y_S=\frac{M}{2}x\sin\theta^*\sin\varphi^*+p_{qy}\left[1-\frac{x}{2}(1+\cos\theta^*)\right]$$
$$+p_{\bar{q}y}\left[1-\frac{x}{2}(1-\cos\theta^*)\right]\ , \qquad \text{(B7)}$$

$$P^z_S=-\frac{x}{2}E\cos\theta^*+\frac{P_L}{2}(2-x)\ , \qquad \text{(B8)}$$

$$P^0_S=\frac{E}{2}(2-x)-\frac{x}{2}P_L\cos\theta^*\ . \qquad \text{(B9)}$$

If we set $P_S=p'_1+p'_2$, we get an explicit expression for $\delta^{(4)}(Q-(p'_1+p'_2))$ involved in Eq. (9).

*Permanent address: Centre de Physique Théorique, CNRS, Marseille, France.

[1]S. D. Drell and T. M. Yan, Phys. Rev. Lett. 25, 316 (1970); Ann. Phys. (N.Y.) 66, 578 (1971).
[2]J. K. Yoh *et al.*, Phys. Rev. Lett. 41, 684 (1978); A. S. Ito *et al.*, Phys. Rev. D 23, 604 (1981).
[3]G. Altarelli, G. Parisi, and R. Petronzio, Phys. Lett. 76B, 351 (1978); 76B, 356 (1978); K. Kajantie and R. Raitio, Nucl. Phys. B139, 72 (1978); F. Halzen and D. N. Scott, Phys. Rev. D 18, 3378 (1978).
[4]Y. L. Dokshitzer, D. I. Dyakonov, and S. I. Troyan, Phys. Lett. 79B, 269 (1978); K. Kajantie and J. Lindfors, Nucl. Phys. B146, 465 (1978).
[5]G. Parisi and R. Petronzio, Nucl. Phys. B154, 427 (1979).
[6]J. Lefrancois, in *High Energy Physics—1980,* proceedings of the XXth International Conference, Madison, Wisconsin, edited by L. Durand and L. G. Pondrom (AIP, New York, 1981), p. 1318.
[7]J. Abad and B. Humpert, Phys. Lett. 80B, 286 (1979); B. Humpert and W. L. Van Neerven, Phys. Lett. 84B, 327 (1979); 85B, 293 (1979); 89B, 69 (1979); Nucl. Phys. 184B, 225 (1981); G. Altarelli, R. K. Ellis, and G. Martinelli, Nucl. Phys. B157, 461 (1979); J. Kubar and F. E. Paige, Phys. Rev. D 19, 221 (1979); J. Kubar, M. Le Bellac, J. L. Meunier, and G. Plaut, Nucl. Phys. B175, 251 (1980).
[8]G. Parisi, Phys. Lett. 90B, 295 (1980); G. Curci and M. Greco, Phys. Lett. 92B, 175 (1980); 102B, 280 (1981).
[9]E. L. Berger and S. J. Brodsky, Phys. Rev. Lett. 42, 940 (1979).
[10]K. J. Anderson *et al.*, Phys. Rev. Lett. 43, 1219 (1979).
[11]G. Preparata, Phys. Rev. D 7, 2973 (1973); G. Preparata, in *Lepton and Hadron Structure*, edited by A. Zichichi (Academic, New York, 1975), p. 54.
[12]A. Chodos, R. L. Jaffe, K. Johnson, C. B. Thorn, and

V. F. Weisskopf, Phys. Rev. D 9, 3471 (1974); P. Hasenfratz and J. Kuti, Phys. Rep. 40C, 75 (1978).
[13]For a recent review, see G. Preparata, in *The Whys of Subnuclear Physics,* proceedings of the International School of Subnuclear Physics, Erice, 1977, edited by A. Zichichi (Plenum, New York, 1979), p. 727.
[14]P. Castorina, G. Nardulli, and G. Preparata, Nucl. Phys. B163, 333 (1980).
[15]P. Castorina, G. Nardulli, and G. Preparata, Phys. Lett. 93B, 291 (1980).
[16]P. Castorina, G. Nardulli, and G. Preparata, Phys. Lett. 90B, 301 (1980).
[17]P. Castorina, G. Nardulli, and G. Preparata, Nucl. Phys. B181, 208 (1981).
[18]G. Preparata and G. Rossi, Nucl. Phys. B111, 111 (1976).
[19]G. Preparata and G. Valenti, Nucl. Phys. B183, 53 (1981); Phys. Rev. Lett. 47, 891 (1981).
[20]G. Valenti (private communication).
[21]J. Badier *et al.*, Report No. CERN-EP/80-150, 1980 (unpublished).
[22]Although data from Ref. 2 are given in a finite rapidity range it is possible to define a mean rapidity $\langle y \rangle$ for each energy of the beam.
[23]C. Kourkoumelis *et al.*, Phys. Lett. 91B, 475 (1980).
[24]G. Curci, M. Greco, and Y. Srivastava, Phys. Rev. Lett. 43, 834 (1979); Nucl. Phys. B159, 451 (1979).
[25]J. C. Collins and D. E. Soper, Nucl. Phys. B193, 381 (1981).
[26]P. Chiappetta and M. Greco, Phys. Lett. 106B, 219 (1981); Nucl. Phys. B199, 77 (1982).
[27]R. K. Ellis, G. Martinelli, and R. Petronzio, Phys. Lett. 104B, 45 (1981); Report No. CERN-TH.3186, 1981 (unpublished).
[28]L. Anderson *et al.*, CERN-Palaiseau-Strasbourg-Zürich Collaboration (NA10 experiment) (unpublished).
[29]CERN-Lausanne-Michigan-Rockefeller Collaboration, CERN Reports Nos. SPSC/80-63, SPSC/P148, 1980 (UA6 experiment) (unpublished).